ROYAL SOCIETY
OF **CHEMISTRY**

PAPER
Aleksandra Jankowska *et al.*
Low-temperature NO conversion with NH$_3$ over
cerium-doped MWW derivatives activated with
copper species

PAPER

Low-temperature NO conversion with NH₃ over cerium-doped MWW derivatives activated with copper species†

Aleksandra Jankowska, [iD] *[a] Klaudia Fidowicz,[a] Małgorzata Rutkowska,[a] Andrzej Kowalczyk, [iD] [a] Marek Michalik[b] and Lucjan Chmielarz [iD] [a]

Silica–alumina MCM-22 zeolite and its cerium-doped analogue (Ce-MCM-22) were obtained by one-pot synthesis. Additionally, the layered precursor of Ce-MCM-22 was subjected to delamination and pillaring procedures, resulting in the formation of Ce-ITQ-2 and Ce-MCM-36, respectively. The obtained micro- and micro-mesoporous supports were modified with copper cations by the ion-exchange method and tested as catalysts for NO conversion with ammonia. The zeolitic samples were characterized with respect to their chemical composition (ICP-OES), texture (low-temperature N₂-sorption), structure (XRD, FT-IR, UV-vis-DR), surface acidity (NH₃-TPD) and reducibility (H₂-TPR). Cu-functionalized zeolites were found to be active and selective catalysts for the selective catalytic reduction of nitrogen oxides with ammonia (NH₃-SCR) in the low-temperature range, effectively operating between 225 and 375 °C. The influence of bimodal porosity on the catalytic efficiency was observed when the space velocity of the reaction increased. The samples doped with cerium were more active than copper-modified silica–alumina MCM-22 in the process of NO-to-NO₂ oxidation, which is an important step in the fast-SCR process. The synergistic interaction of cerium–copper species together with a more open structure of the delaminated copper-modified sample (Cu–Ce-ITQ-2) influenced its activity in low-temperature NO conversion under humid reaction conditions.

Introduction

The excessive emission of gaseous nitrogen compounds, including nitrogen oxides, NO_x = NO and NO_2, is one of the most serious issues that negatively affects the ecosystem and human health. The impact on the aforementioned areas is manifested, among others, by ozone layer depletion and acid rain.[1] In turn, living organisms, including humans, suffer the most from serious systemic diseases, mainly related to the respiratory system, caused by the action of nitrogen oxides.[1] The release of NO_x into the atmosphere occurs as a result of emissions from stationary (*e.g.*, coal-fired power plants) and mobile (*e.g.*, vehicle traffic) sources. Nevertheless, nitrogen oxides are predominantly produced by high-temperature combustion processes. In stationary sources, NO_x abatement is most frequently achieved by the application of selective catalytic reduction of nitrogen oxides with ammonia (NH₃-SCR) occurring in the presence of commercial monolithic V_2O_5–TiO_2 catalysts.[2,3] The vanadia–titania system demonstrates the effective conversion of NO_x within a specific temperature ranging from 300 to 400 °C in high-dust streams. This relatively narrow temperature range of effective operation makes the V_2O_5–TiO_2 catalyst unsuitable for use in modern industrial units, where NO_x should be reduced by ammonia to N_2 below 300 °C.[4] Such a requirement is necessary for the retrofitting of NH₃-SCR systems operating with low-dust and desulfurized gas stream.[5] The rearrangement of the SCR installation, from high-dust to low-dust configuration, is based on the positioning of the catalytic SCR section down-stream of the gas cleaning system. This sequence of gas purification modules is designed to remove dust and sulphur oxides prior to the conversion of NO_x in the SCR unit. The electrostatic precipitator, used for gas dedusting, operates at 250 °C, or even lower temperature. Thus, the implementation of the NH₃-SCR system for low-dust streams needs the development of low-temperature catalysts for NO conversion.

Transition metals are characterized by the direct gaining and release of electrons within the d shell, thus it may account for their effortless redox properties.[4] Hence, the potential catalysts for application in the NO_x conversion

[a] *Faculty of Chemistry, Jagiellonian University in Kraków, Gronostajowa 2, 30-387 Kraków, Poland. E-mail: aleksandra1.jankowska@uj.edu.pl*
[b] *Institute of Geological Sciences, Jagiellonian University in Kraków, Gronostajowa 3a, 30-387, Kraków, Poland*

process are frequently based on transition metal (TM) modified porous supports. Among them, TM-exchanged zeolites,[6,7] mainly those modified with copper,[8,9] iron[8,10] or manganese[8,11] are under high scientific interest. Considering the low-temperature NH_3-SCR activity of d-shell ions, copper-modified catalysts efficiently facilitate NO_x conversion in the low-temperature region.[4] Another interesting aspect that should be considered in the design of catalysts is the improvement of their activity by promoters, *e.g.*, rare earth elements (mainly lanthanides). Lanthanides seem to be good candidates to play this role due to various possible oxidation states and economical pricing. Moreover, the addition of a small amount of cerium or lanthanum can enhance the overall acid site content, facilitating the adsorption of reactive gases and subsequently boosting its effectiveness in catalytic processes.[12] In recent years, the systems based on the interaction of copper and cerium have attracted great interest as a combination that has a beneficial effect on low-temperature NO conversion.[13–16] The increased catalytic activity of such systems is related to promoting electron transfer facilitating the rapid oxidation of NO to NO_2, thus driving the fast-SCR process.[17] The fast-SCR reaction (NO + NO_2 + $2NH_3$ → $2N_2$ + $3H_2O$) is considered to be the most probable low-temperature way of nitrogen(II) oxide conversion.[18] Thus, catalytic systems for potential application in the NH_3-SCR process operating below 250 °C should be effective in the formation of reactive nitrogen(IV) oxide.

The selection of the supports for the deposition of the active phase is equally important for the efficient conduction of the catalytic reaction. As previously mentioned, TM-modified alumina–silica supports show a high research value in the context of NO_x into N_2 transformation. Among aluminosilicates, zeolites are one of the most significant materials with high industrial potential. The 'Big Five' zeolite families show network types of BEA, FAU, FER, MFI, and MOR, which are widely utilized in large-scale processes.[19] Nevertheless, MCM-22, a zeolite of the MWW family, is another interesting type of structure, which finds particular application in the processes of hydrocarbon conversion, *e.g.*, the synthesis of monoalkyl benzenes.[20] MCM-22 is also a great example of 2D zeolites characterized by repeated individual sheets with a layer thickness of 2.5 nm.[21] This layered arrangement of MWW sheets determines the value of this material and its potential modifications leading to structures with bimodal porosity. The presence of an additional porous system enables improved access to the active centres of zeolites, which is a crucial factor in converting bulkier molecules.[21] The products of MCM-22 precursor transformation form pillared (MCM-36) or delaminated (ITQ-2) derivatives with decreased diffusion limitations and increased mass transfer because of a more open porous structure. The modified MWW micro-mesoporous zeolites functionalized with transition metals were found to be active and selective catalysts in the NH_3-SCR process.[22–24] In this regard, Rutkowska *et al.* showed the effective low-temperature catalytic operation of copper-

modified ITQ-2 in terms of activity and hydrothermal stability in NO conversion.[22] Therefore, these findings make the selected catalytic system interesting for further research.

The presented studies are focused on low-temperature NH_3-SCR catalyst development for application in retrofitted NO conversion systems operating with low-dust and desulfurized gas stream. Herein, we reported the synthesis of cerium-doped MWW derivatives activated with copper cations, their catalytic performance in the NH_3-SCR process and possible synergistic interactions between cerium and copper species. The properties of micro-mesoporous zeolites, especially the house-of-cards ITQ-2 structure, with relatively wide channels should facilitate efficient internal diffusion of reactants. Moreover, the incorporation of cerium into the zeolite structure may increase catalytic efficiency as a result of the fast-SCR process. Therefore, these catalytic systems provide certain advantages for designing effective catalysts of the NH_3-SCR process.

Experimental methods

Catalyst preparation

Synthesis of 2D MCM-22 precursors and their calcined forms. The layered form of the aluminum–silicon MCM-22 parent material, denoted as Al-MCM-22(P), was obtained based on the synthesis procedure described by Corma *et al.*[25] The synthesis gel was composed of sodium hydroxide (NaOH, Honeywell), sodium aluminate (NaAlO₂, Sigma-Aldrich), fumed silica (SiO₂, Aerosil 200), hexamethyleneimine (HMI, Aldrich) and deionized water. The molar composition of the ingredients in the reaction mixture was as follows: $SiO_2 : Al_2O_3 = 30$, $OH : SiO_2 = 0.30$, $Na : SiO_2 = 0.30$, $HMI : SiO_2 = 0.90$, $H_2O : SiO_2 = 40$. In the first step of the synthesis, NaOH and NaAlO₂ were dissolved in distilled water, and then HMI and SiO₂ were subsequently added to the obtained mixture. The prepared suspension was stirred for 2 h to homogenize its components. Afterwards, the slurry was transferred to a PTFE-lined stainless-steel autoclave (150 mL) and hydrothermally treated at 150 °C for 7 days. After one week, the autoclave was quenched in a cooling bath, while the obtained slurry was filtered, and the obtained material was washed with deionized water (pH ∼ 7). The Al-MCM-22(P) sample was dried at 60 °C for 15 h and then calcined at 550 °C for 6 h (with a heating rate of 1 °C min⁻¹ from RT to 550 °C) in an oxidizing atmosphere.

The second 2D material, cerium–aluminum–silicon MCM-22, named Ce-MCM-22(P), was synthesized according to Roth *et al.*[26] The molar composition of the reaction gel was equal to $0.01Ce : SiO_2 : 0.25NaOH : 0.033Al_2O_3 : 0.6HMI : 20H_2O$, while the used chemical reagents were the same as in the case of the previously described material. The only exception is the addition of cerium(III) nitrate (Ce(NO₃)₃·6H₂O, Acros Organics) and hydrochloric acid (HCl, Honeywell), although the content of acid and nitrate anion was insignificant.

This journal is © The Royal Society of Chemistry 2025

Catal. Sci. Technol., 2025, **15**, 1456–1472 | **1457**

Hence, they were not taken into account in calculations of the total synthesis mixture composition.[26]

The preparation of the synthesis gel started with the dissolution of cerium salt in an HCl solution (0.3 mol L^{-1}). Then, the fumed silica was added to the system and subsequently, the obtained mixture was heated up to 90 °C and stirred for 2 h under reflux. After cooling down of the solution, the organic template (HMI) was dropwise added, and the mixture was mixed with a water solution of NaOH and NaAlO$_2$. The formed gel was well stirred at room temperature for 20 h and then moved to a PTFE-lined stainless-steel autoclave (100 mL). The zeolite crystallization under hydrothermal static conditions was conducted at 165 °C for 6 days. Then, the material was recovered, dried and partially calcined, similar to the previously described aluminum–silicon parent zeolite. The obtained template-free material was denoted as Ce-MCM-22. However, the major part of the layered precursor, Ce-MCM-22(P), was subjected to the further modifications described below.

Swelling – preparation of Ce-MCM-22(S). The swelling procedure of the layered cerium precursor to obtain a swollen zeolite, referred to as Ce-MCM-22(S), was a necessary step to prepare delaminated (Ce-ITQ-2) and pillared (Ce-MCM-36) structures. The modification was based on the use of ion-exchanged bromides of hexadecyltrimethylammonium (CTMABr, Sigma-Aldrich) and tetrapropylammonium aqueous solution (TPABr, Sigma Aldrich). For the modification of 5 g of layered Ce-MCM-22(P), a solution composed of 100 g of CTMA$^+$Br$^-$/OH$^-$ (~70% ion-exchange, ~25 wt%), 30 g of TPA$^+$-Br$^-$/OH$^-$ (~70% ion-exchange, ~35 wt%) and 30 g deionized water was used. The obtained mixture was stirred under reflux at 80 °C for 16 h. Afterwards, the swollen zeolite was used for the synthesis of delaminated and intercalated samples.

Delamination – preparation of Ce-ITQ-2. The delayered Ce-MCM-22(P) zeolite was produced according to the procedure described in the literature.[27] The sample was obtained by the treatment of the swelling Ce-MCM-22(P) suspension in an ultrasound bath (300 W, 45 kHz, EMAG) for 1 h. Subsequently, the mixture was acidified by dropwise addition of concentrated hydrochloric acid (HCl, Honeywell) to get pH ~ 2. The sample, denoted as Ce-ITQ-2(P), was centrifuged, washed with deionized water, dried at 60 °C for 15 h and finally calcined at 550 °C for 6 h (with a heating rate of 1 °C min^{-1} from RT to 550 °C) in air. The applied procedure resulted in the formation of Ce-ITQ-2 zeolite.

Intercalation – preparation of Ce-MCM-36. The swollen Ce-MCM-(S) sample was centrifuged, washed with deionized water and dried (60 °C, 15 h) and then intercalated with silica pillars.[22] The sample containing the organic matrix is named Ce-MCM-36(P). The Ce-MCM-22(S) pillaring procedure included: mixing the sample with tetraethyl orthosilicate (TEOS, Sigma-Aldrich) using a mass ratio of 1:5 (solid : liquid), then heating up to 80 °C and stirring under an argon atmosphere for 24 h. Afterwards, the material was separated by filtration, washed thrice with acetone and ethanol and

later dried at 60 °C for 15 h. Subsequently, the solid product was hydrolysed in deionized water with a weight proportion of 10 g H$_2$O per 1 g of zeolite at 80 °C for 24 h. Then, the slurry was filtered, washed with distilled water, dried at 60 °C for 15 h and finally air-calcined at 550 °C for 6 h (with a heating rate of 1 °C min^{-1} from RT to 550 °C), resulting in the Ce-MCM-36 sample.

Functionalization of zeolites by the ion-exchange method. The as-synthesized zeolites (Al-MCM-22, Ce-MCM-22, Ce-ITQ-2, Ce-MCM-36) were subjected to a triple ion-exchange procedure with a 0.5 mol L^{-1} solution of ammonium nitrate (NH$_4$NO$_3$, Sigma-Aldrich) to obtain ammonium forms of zeolites. For every treatment, the liquid : solid ratio of 1 wt : 80 wt was used. The obtained mixtures were refluxed at 80 °C for 1 h. The resulting solids were filtered, washed with distilled water, dried at room temperature and calcined at 550 °C for 6 h (with a heating rate of 1 °C min^{-1} from RT to 550 °C) in an air atmosphere. The samples were ion-exchanged under reflux at 85 °C for 6 h with Cu(COOCH$_3$)$_2$·H$_2$O solution (0.06 mol L^{-1}, Chempur), using a liquid to zeolite ratio of 80 mL g^{-1}. After that, the samples were filtered, washed with distilled water, dried at 60 °C for 15 h and finally calcined at 550 °C for 6 h (with a heating rate of 1 °C min^{-1} from RT to 550 °C) in an air atmosphere. The copper-modified samples were denoted as Cu-Al-MCM-22, Cu-Ce-MCM-22, Cu-Ce-ITQ-2 and Cu-Ce-MCM-36.

Catalyst characterization

Powder XRD (P-XRD) analysis was carried out using a Bruker D2 Phaser Tabletop X-ray diffractometer with CuKα (λ = 1.54184 Å) radiation. Data were collected stepwise over two angular regions, with steps of 0.02° 2θ. The analysed regions were as follows: 2θ ranges of 1–11° and 5–40° with a counting time of 5 s and 1 s per step, respectively.

SEM images were obtained using a scanning electron microscope HITACHI SU8600 equipped with an X-ray energy dispersive spectrometer Bruker XFlash 7. Both for imaging and chemical analysis, an accelerating voltage of 20 kV was used. The secondary electron signal (upper and lower detector) was applied in observations of the morphology of material particles.

The analysis of Si, Al, Ce and Cu content in the studied samples was done by inductively coupled plasma optical emission spectrometry (ICP-OES) on an iCAP 7400 instrument (Thermo Scientific). The analysed samples were dissolved in a mixture composed of 6 mL HNO$_3$ (Honeywell, 67–69%), 2 mL HCl (Honeywell, 30%) and 2 mL HF (Honeywell, 47–51%) using a microwave digestion system at 190 °C for 2 h (Ethos Easy, Milestone).

FTIR spectra of the samples were recorded using a Nicolet 6700 spectrometer (Thermo Scientific) equipped with a DRIFT (diffuse reflectance infrared Fourier transform) accessory and DTGS detector. Dried samples were ground with dried potassium bromide powder (sample concentration in KBr – 4 wt%). The measurements were carried out in the

1458 | *Catal. Sci. Technol.*, 2025, **15**, 1456–1472

This journal is © The Royal Society of Chemistry 2025

wavenumber range of 400–1400 cm^{-1} with a resolution of 4 cm^{-1}.

The textural parameters of the samples were determined by N$_2$ sorption at −196 °C using a 3Flex (Micromeritics) automated gas adsorption system. Before every analysis, the samples were outgassed under vacuum conditions at 350 °C for 24 h. The specific surface area (S_{BET}) of the samples was determined using the BET equation. The micropore volume and external surface area were calculated using t-plot analysis, while the mesopore volume was calculated from the adsorption branch of the isotherm using the BJH model.

The UV–vis–DR spectra of the Ce and Cu-modified samples were recorded in the wavelength range of 190–900 nm with a resolution of 2 nm applying a Lambda 650S spectrometer (Perkin Elmer).

Temperature-programmed reduction of the samples with hydrogen (H$_2$-TPR) was used to analyse the reducibility of the metal species deposited on supports. The experiment was carried out in a fixed-bed flow microreactor system equipped with a thermal conductivity detector (TCD, Valco). Before each H$_2$-TPR run, 25 mg of the sample (particle size in the range of 160–315 μm) was placed in the reactor and degassed in a flow of pure argon at 550 °C for 20 min. Subsequently, the system was cooled to 80 °C and the temperature-programmed reduction process was started. In the H$_2$-TPR process, the catalyst was reduced in a flow of 5 vol% H$_2$/Ar (10 mL min^{-1}) in the temperature range of 100–900 °C with a linear heating rate of 10 °C min^{-1}.

Temperature-programmed desorption of ammonia (NH$_3$-TPD) was used to determine the acidity of the samples. The measurements were performed in a flow quartz microreactor system equipped with a quadrupole mass spectrometer (QMS) used as a detector (PREVAC). The flow rate of the gas mixture was adjusted and controlled by mass flow controllers (Brooks Instrument). Prior to each study, 50 mg of the sample was outgassed in a flow of pure helium at 600 °C for 30 min. Subsequently, the microreactor was cooled to 70 °C and the sample was saturated in a flow of a gas mixture containing 1 vol% NH$_3$ diluted in helium for about 2 h. Then, the catalyst was purged in helium flow until a constant baseline level was attained. Ammonia desorption was carried out with a linear heating rate of 10 °C min^{-1} in a flow of pure He (20 mL min^{-1}). Calibration of QMS with the calibration mixture allowed recalculation of the detector signal into the rate of ammonia desorption.

Catalytic studies

Selective catalytic reduction of NO with ammonia (NH$_3$-SCR). NH$_3$-SCR catalytic studies were performed in the experimental system consisting of a flow fixed-bed quartz microreactor with the outlet connected directly to the detector – quadrupole mass spectrometer –QMS (PREVAC). The used gas mixture contained 0.25 vol% NO, 0.25 vol% NH$_3$, 2.5 vol% O$_2$ and optionally 5 vol% H$_2$O diluted in helium (total flow rate of 40 mL min^{-1}). Before the catalytic

test, 25 or 100 mg of the sample (particle size in the range of 160–315 μm) was placed in a quartz microreactor and outgassed in the flow of helium at 550 °C for 30 min. Afterwards, the microreactor was cooled to 100 °C and the catalytic test was initiated with a linear heating rate of 10 °C min^{-1}, in the temperature range of 100–400 °C. Catalytic tests were performed under atmospheric pressure.

Moreover, for the selected catalyst, the isothermal stability tests were done at 225 °C for 20 h with using a dry (without water vapour addition) or wet (5 vol% H$_2$O) reaction mixture. Both tests were done for 100 mg of catalyst (particle size in the range of 160–315 μm), under atmospheric pressure.

Ammonia oxidation

The catalyst mass, particle size, equipment and outgassing procedure for the ammonia oxidation studies were the same as in the case of the NH$_3$-SCR process. The process of ammonia oxidation was studied in the range of 100–550 °C under atmospheric pressure. A gas mixture containing 0.5 vol% NH$_3$ and 2.5 vol% O$_2$ diluted in helium (total flow rate of 40 mL min^{-1}) was used.

NO to NO$_2$ oxidation

The studies of catalytic NO to NO$_2$ oxidation were carried out in the same system as the NH$_3$-SCR tests. The reaction was studied in a flow of gas mixture containing 0.5 vol% NO and 2.5 vol% O$_2$ diluted in He (total flow rate of 40 mL min^{-1}). The FTIR spectrometer Nicolet iS5 (Thermo Scientific), equipped with a gas cell of 10 cm in length, operating in the wavenumber range of 625–4000 cm^{-1} and with a resolution of 4 cm^{-1}, was used for the analysis of the reaction mixture down-stream as well as up-stream of the microreactor. The absorption bands at 1593 cm^{-1} and 1912 cm^{-1} were used for the analysis of nitrogen(IV) oxide and nitrogen(II) oxide, respectively.

Results and discussion

Powder X-ray (P-XRD) patterns of layered MCM-22 derivatives recorded in the low- and high-angle range are presented in Fig. 1A and B, respectively. The analysis of the P-XRD diffractogram obtained for the alumina–silica Al-MCM-22(P) sample (Fig. 1) shows the presence of reflections characteristic of the MWW structure. Reflections (001)[21] located approximately at 3.2° 2θ and (002)[21] at about 6.6° 2θ prove that the MWW sheets are vertically aligned, while the average separation between two neighbouring layers relates to 2.85 nm (the sum of the layer thickness and the inter-layer distance – space occupied by the organic template).[21] Preservation of the MWW structure is manifested by the presence of intra-layer reflection (100) at 7.2° 2θ, corresponding to the structure of the individual zeolite sheet, as well as other (hk0) reflections characterized by higher values of 2θ degrees (Fig. 1B).[22] The same indicative reflections were found for the layered precursor containing
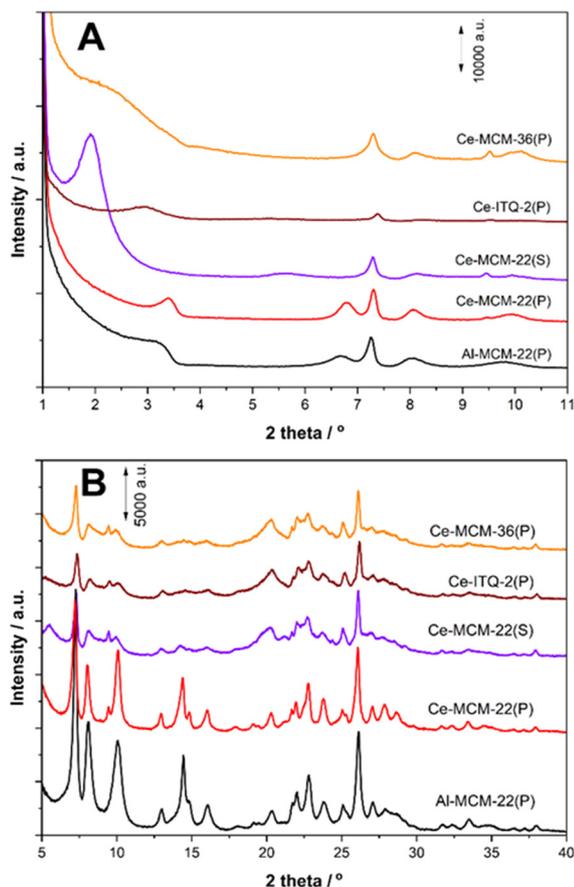
This journal is © The Royal Society of Chemistry 2025

Catal. Sci. Technol., 2025, **15**, 1456–1472 | 1459

Fig. 1 P-XRD diffractograms recorded for the Al-MCM-22 and Ce-MWW supports before calcination at (A) low- and (B) high-angle ranges.

Fig. 2 P-XRD diffractograms recorded for the Al-MCM-22 and Ce-MWW supports after calcination at (A) low- and (B) high-angle ranges, as well as diffractograms of their Cu-modified derivatives (C) in the high-angle range.

cerium, Ce-MCM-22(P) (Fig. 1A and B), confirming the successful synthesis of the 2D material. The only additional reflection, located at about 9.5° 2θ, observed for all obtained Ce-MWW derivatives is possibly related to the presence of small amounts of impurities.[26]

In the case of Ce-MCM-22(S), the swelling process caused a shift of the (001) and (002) reflections towards lower angle values (1.9° and 5.6° 2θ, respectively), indicating an expansion of the interlayer distance from 0.3 to 2.1 nm. The increase in the layers' separation distance is related to the introduction of organic surfactants into the area linking the MWW sheets. On the other hand, the calcination process, based on the removal of the organic templates, performed for the as-synthesized layered precursors, resulted in the disappearance of the (00l) reflections for Al- and Ce-MCM-22 precursors (Fig. 2A and B). This phenomenon indicates topotactic transformation from the 2D to 3D microporous structure of Al-MCM-22 and Ce-MCM-22. At the same time, the (100) reflection remained unchanged pointing out that the samples have the MWW-ordered matrix after thermal treatment.

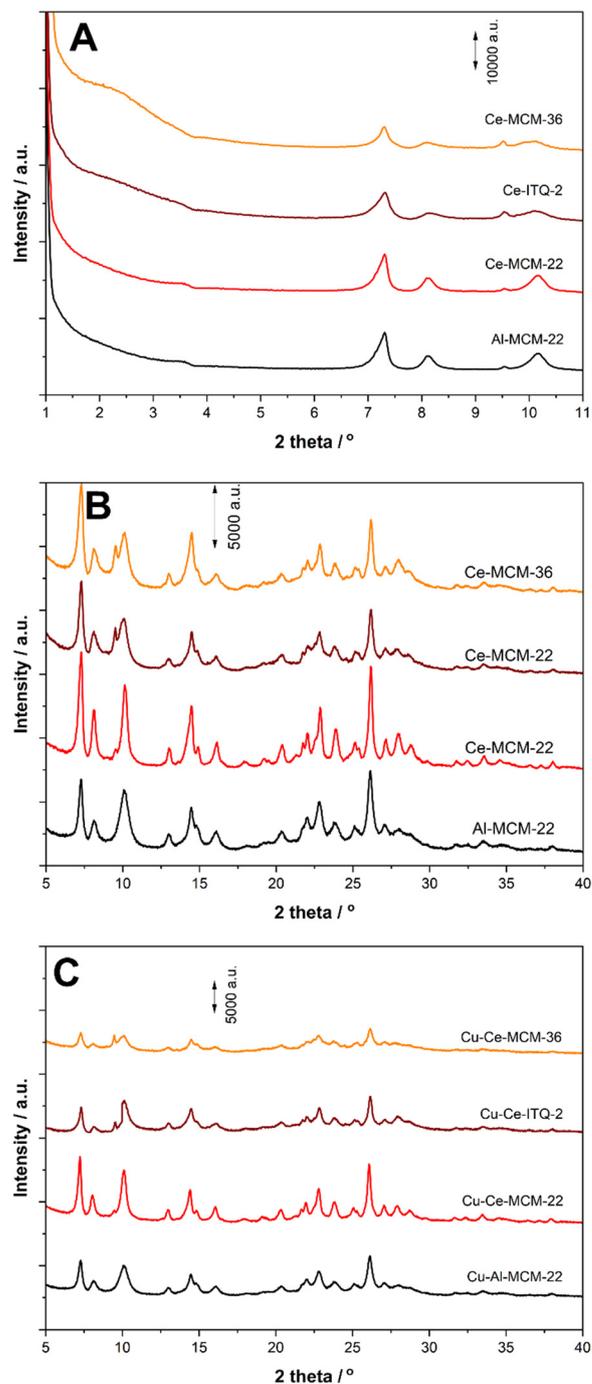For the Ce-ITQ-2 and Ce-MCM-36 samples, both before (Fig. 1A and B) and after organic template oxidation

(Fig. 2A and B), the (002) reflection is absent for Ce-ITQ-2 or slightly visible for Ce-MCM-36. It suggests that the framework of zeolite was delaminated (Ce-ITQ-2) – as a result of swelling and ultrasound treatment or partially pillared (Ce-MCM-36) – due to the partial intercalation with silica of the previously swollen zeolite precursor. What is more, the decrease in reflection intensity, observed for the delaminated and

1460 | *Catal. Sci. Technol.*, 2025, **15**, 1456–1472

This journal is © The Royal Society of Chemistry 2025

pillared samples (Fig. 2B), indicates a slightly less ordered zeolite structure in contrast to Ce-MCM-22.

Modification of porous supports with copper cations did not result in the altering of the MWW matrix (Fig. 2C). All reflections characteristic of this type of framework can be observed for the obtained Cu-exchanged zeolites, which suggests that the applied modification method did not influence the zeolite structure. Moreover, copper species were well-dispersed on the surface of zeolites owing to the lack of reflections characteristic of copper oxides.

The SEM images together with maps of element distribution were recorded for copper modified samples. Results obtained for the Cu–Al-MCM-22 sample are presented in Fig. S1,† while images of copper-containing Ce-MWW derivatives are shown in Fig. 3. In the case of the Cu–Al-

MCM-22 catalyst (Fig. S1A†), the size and shape of zeolite crystals is non-uniform, with diameter ranging between 30 and 120 μm. For the Cu–Ce-MCM-22 sample (Fig. 3A) the crystal morphology is homogeneous, with a particle size of approximately 6 μm and biconcave disk shape. The form of delaminated and pillared copper modified samples changed after applied modifications. In the case of the Cu–Ce-ITQ-2 sample (Fig. 3B), randomly arranged zeolite layer packets can be observed, which are the result of the used delamination process. For the Cu–Ce-MCM-36 catalyst (Fig. 3C), uniform zeolite crystals can be found, although part of them are covered by the amorphous silica formed due to the modification with TEOS. As can be seen from imaging maps (Fig. S1B and C and 3A–C† (1–3)), aluminum, cerium and copper species are well dispersed in the silica matrix of zeolite. However, in the case of all the samples, a small part
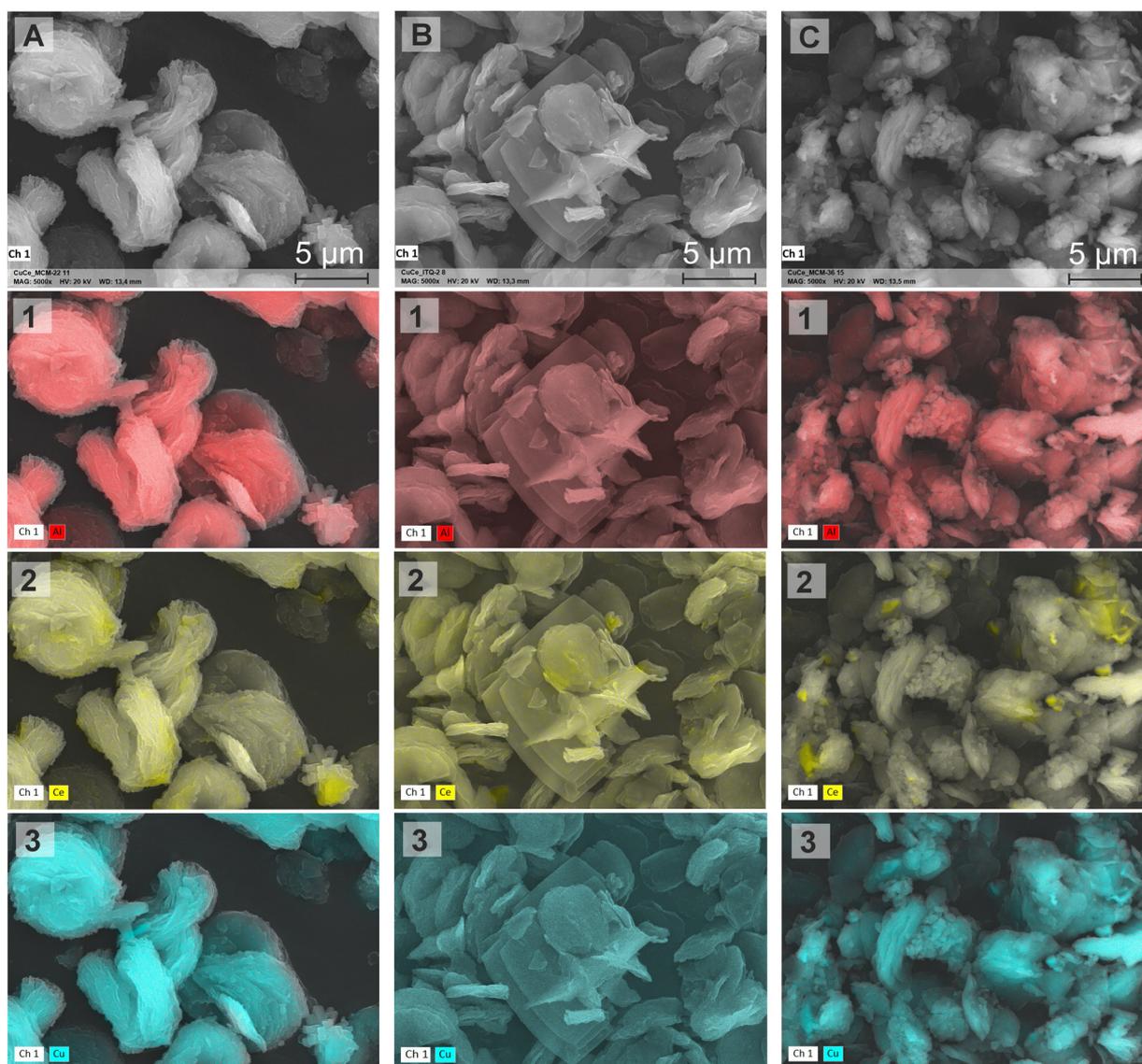

Fig. 3 SEM images of Cu–Ce-MCM-22 (A), Cu–Ce-ITQ-2 (B) and Cu–Ce-MCM-36 (C) samples and SEM micrographs with EDX maps of element distribution: aluminium (1), cerium (2) and copper (3).

This journal is © The Royal Society of Chemistry 2025

Catal. Sci. Technol., 2025, **15**, 1456–1472 | **1461**

of cerium forms slightly more aggregated species located outside of the porous structure.

The structure of zeolite materials, both before and after the calcination, was examined by FT-IR using DRIFT mode (Fig. 4). The bands observed for alumina–silica zeolite, Al-MCM-22(P) and Al-MCM-22, were recognized as typical of the MWW structure.[28] For these samples, v_{asym} stretching T–O internal ($\sim$1090 cm^{-1}) and external ($\sim$1245 cm^{-1}), as well as v_{sym} stretching T–O internal ($\sim$740 cm^{-1}) and external ($\sim$810 cm^{-1}) vibrations were found for template-containing (Fig. 4A) and template-free (Fig. 4B) zeolite materials.[28] What is more, the band related to v_{asym} (Si–O–Si) stretching was shifted from 1085 cm^{-1} (for alumina–silica zeolite) to about 1078 cm^{-1} after modifications with Ce^{3+} cations (Fig. 4A). According to Wu *et al.*[29] this shift towards lower wavenumbers can be considered as evidence of introducing cerium cations into the MWW framework. For the thermal-treated zeolites, Fig. 4B, the same effect was observed. Additionally, other peaks, located at about 455 cm^{-1}, characteristic of T–O bending vibrations, and around 555 cm^{-1}, assigned to Al–O–Si deformation modes, were identified in the spectra of the analysed samples (Fig. 4). The intensity of these bands decreased for the modified-layered

derivatives, Ce-ITQ-2 and Ce-MCM-36, compared to zeolites with 3D structures. This phenomenon resulted possibly from the less ordered structure of MWW derivatives, which is consistent with powder XRD results.[30]

The porosity of the MCM-22-derived samples was analysed by low-temperature N$_2$ adsorption–desorption measurements. Fig. 5A shows the N$_2$ adsorption–desorption isotherms recorded for silica–alumina and silica–alumina–ceria precursors, while Fig. 5B depicts isotherms recorded for the copper-modified zeolite materials. Isotherms obtained for Al-MCM-22 and Ce-MCM-22 can be classified as representative for microporous materials – type I according to IUPAC classification.[31] The H4 hysteresis loop observed for Ce-ITQ-2 (presented in Fig. 5B) indicates that the sample belongs to a micro-mesoporous type of material.[32] The N$_2$ adsorption–desorption isotherm of Ce-MCM-36, Fig. 5A, is similar to that recorded for the Ce-MCM-22 sample. Nonetheless, above the relative pressure of 0.02, a systematic increase in the adsorbed volume of N$_2$ can be observed. This growth implies the possible presence of larger pores characterized by inhomogeneous dimensions. For both MWW derivatives, Ce-ITQ-2 and Ce-MCM-36 (Fig. 5A), the applied delamination and intercalation procedure did not destroy their
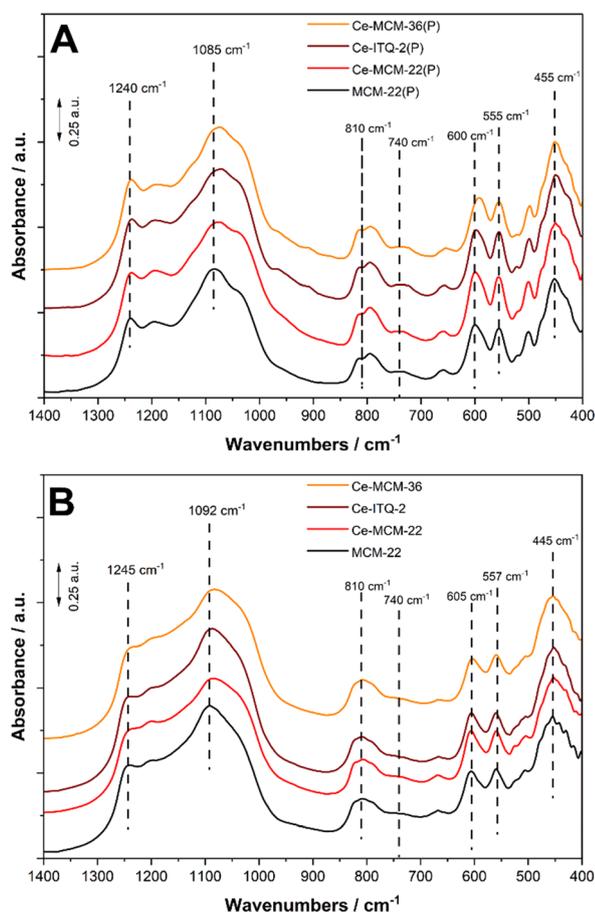

Fig. 4 IR spectra in the DRIFT mode of the Al-MCM-22 and Ce-MWW zeolites before (A) and after (B) calcination.
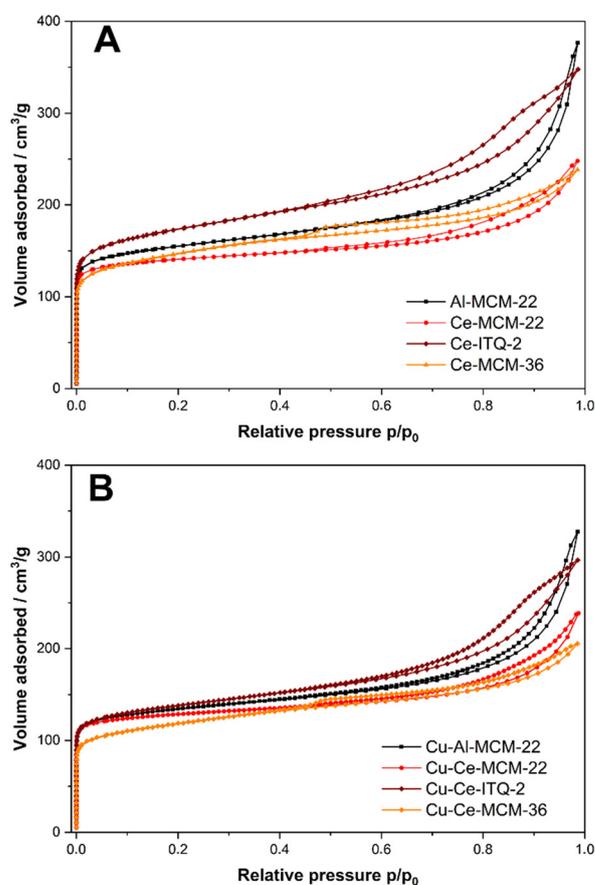

Fig. 5 Nitrogen adsorption–desorption isotherms recorded for the Al-MCM-22 and Ce-MWW supports (A) and their copper-modified forms (B).

1462 | *Catal. Sci. Technol.*, 2025, **15**, 1456–1472

This journal is © The Royal Society of Chemistry 2025

microporous structure. However, for the delaminated zeolite, an increase in N_2 adsorbed volume is higher in the range of the low relative pressure (p/p_0) in comparison to the silica pillared material. It may be connected with the possible micropore clogging by aggregates of amorphous silica in Ce-MCM-36 as a result of the partial intercalation of the zeolite layers. The shape of the N_2 adsorption–desorption isotherms did not change significantly after the deposition of copper species on their surface (Fig. 5B). The only observation is a slight decrease in nitrogen uptake after copper deposition, probably because of the partial blocking of pores by metal oxide aggregates. Apart from that, the samples' porous properties remained consistent after copper deposition.

Table 1 presents the textural parameters (specific surface area – S_{BET}, external surface area – S_{ext} and volume of micro – V_{micro} and mesopores – V_{mezo}) of the zeolitic materials and their Cu-modified forms. The specific surface area and micropore volume determined for 3D Al-MCM-22 and Ce-MCM-22 are similar. The mesopore volume of alumina-MCM-22 is higher in comparison to its ceria analogue, possibly due to the presence of larger pores between zeolite crystals. It is evidenced by the increased nitrogen adsorption step at p/p_0 above 0.80 for Al-MCM-22 (Fig. 5A). Regarding the Ce-ITQ-2 sample, a large increase in the specific surface area and mesopore volume was observed; this phenomenon was not so evident in the case of the pillared sample, possibly due to the embedment of amorphous silica deposits during the incomplete intercalation process. Fig. S0A and B† show the distribution of pore volumes concerning diameters, for the micro- and micro-pore range, respectively. Based on the analysis of the range below 2 nm, the microporous character of the samples was maintained after introduction of additional porous systems (Fig. S0A†). In turn, the generation of mesoporosity in delaminated and intercalated samples was achieved, while the pore diameters are below 4 nm (Fig. S0B†). The textural parameters of MWW-derivatives modified with copper by the ion-exchange method, in general, decreased concerning S_{BET}, micro- and mesopore volume and S_{ext}. These results are most likely related to the clogging of pores and the deposition of small copper oxide forms on the surface of

zeolite crystals. However, these decreases are rather slight (9–20%) and the materials are still characterized by relatively good textural properties.

Table 1 presents the chemical composition (Al, Ce, Cu) of the zeolite samples determined from ICP-OES measurements. The intendent molar ratios of the synthesized materials were as follows, Si/Al = 15, while Si/Ce = 100. The results obtained for Al-MCM-22 and Ce-MCM-22 indicate that the real Si/Al ratios are about 11, while the Si/Ce ratio in the Ce-MCM-22 sample is about 100. Hence, aluminum was preferentially incorporated into the sample compared with silicon, whereas cerium was incorporated into the structure with the intended content. The analysis of the chemical composition of micro-mesoporous analogues of Ce-MCM-22 indicates that aluminum and cerium content decreased as a result of modifications of the material precursor. In the case of the Ce-ITQ-2 sample, the molar ratios of Si/Al are about 12 and Si/Ce ~ 185, while for Ce-MCM-36 the silicon to cerium ratio changed to around 109. It may be connected with severe modification conditions including treatment of the samples in basic (swelling) medium or basic/acidic (swelling/delamination) solutions. Such an approach may result in a partial extraction of silicon, aluminum and cerium from the zeolite matrix and thus influence the chemical composition of materials.

For the samples modified with copper, its content was in the range of 5.3–6.4 wt%, although the correlation between the Si/Al and Si/Ce molar ratios and copper content in the samples of this series was not found, especially, because both aluminum and cerium centres can constitute ion-exchange sites to accumulate copper cations. The coordination and aggregation of the cerium and copper species in MWW zeolites and their modifications were analysed using UV-vis-DR spectroscopy. The spectra recorded for the as-synthesized, calcined and Cu-modified samples are presented in Fig. 6A–C, respectively. For the template-containing materials, two intense absorption peaks can be distinguished (Fig. 6A). The first band, centred at around 200 nm, can be assigned to Ce^{3+} cations, while the second peak, centred at around 300 nm, corresponds to Ce^{4+}, both in tetrahedral coordination. The presence and location of bands characteristic of cerium cations indicate that they were built into the zeolite

Table 1 Textural parameters, chemical composition, concentration and density of acid sites of the MCM-22 and Ce-MWW derivatives and their Cu-modified forms

Sample	S_{BET}^{a} [m² g⁻¹]	V_{micro} [cm³ g⁻¹]	V_{mezo} [cm³ g⁻¹]	S_{ext}^{b} [m² g⁻¹]	Al [wt%]	Ce [wt%]	Cu [wt%]	C_a^{c} [μmol g⁻¹]	D_a^{d} [μmol m⁻²]
Al-MCM-22	588	0.187	0.178	132	3.6	—	—	947	1.61
Ce-MCM-22	551	0.191	0.104	68	3.6	2.0	—	872	1.58
Ce-ITQ-2	645	0.203	0.238	169	3.2	1.1	—	890	1.38
Ce-MCM-36	540	0.211	0.125	75	3.5	1.8	—	1023	1.89
Cu-Al-MCM-22	512	0.164	0.149	105	3.3	—	5.4	438	0.86
Cu-Ce-MCM-22	499	0.172	0.099	66	3.3	1.7	5.3	593	1.19
Cu-Ce-ITQ-2	518	0.156	0.198	140	2.8	1.1	5.8	836	1.61
Cu-Ce-MCM-36	434	0.166	0.118	75	3.3	1.7	6.4	418	0.96

^{a} BET (Brunauer–Emmett–Teller) surface area. ^{b} t-Plot external surface area. ^{c} Concentration of acid sites. ^{d} Density of acid sites.

This journal is © The Royal Society of Chemistry 2025

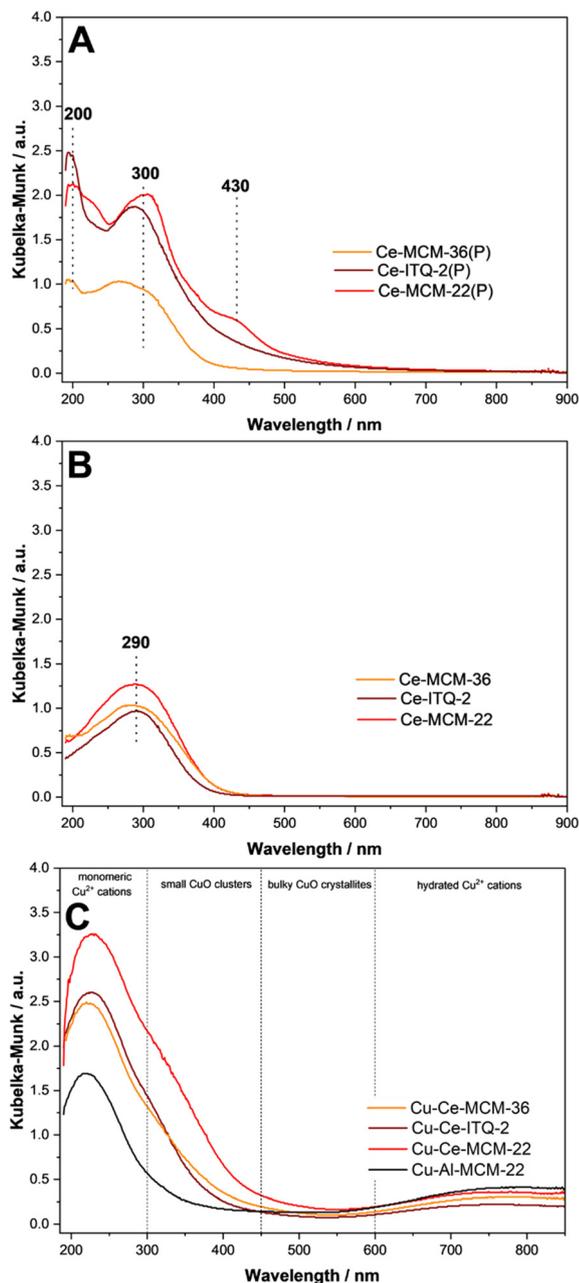*Catal. Sci. Technol.*, 2025, **15**, 1456–1472 | **1463**

Fig. 6 UV-vis-DR spectra recorded for the Ce-MWW derivatives – before (A) and after (B) calcination, as well as spectra recorded for the Cu-modified Al-MCM-22 and Ce-MWW (C).

attributed to the ligand-to-metal charge transfer ($O^{2-} \rightarrow Ce^{4+}$), for a homogeneously distributed tetracoordinated Ce^{4+}.[33] The lack of the band characteristic of Ce^{3+} cations, expected at about 220 nm, is possibly assigned to their partial oxidation to Ce^{4+} under calcination conditions. Hence, the broad absorption band centred at about 290 nm could arise from the coexistence of well-dispersed Ce^{3+} and Ce^{4+} cations. Moreover, the high degree of cerium cation dispersion in the zeolite matrix can be confirmed by the absence of the bands located at higher wavelengths, characteristic of the extra-framework ceria nanocrystallites. The analysis of UV-vis-DR spectra, presented in Fig. 6C, gives information about the Cu and Cu–Ce chemical environment. The pure silica–alumina copper-modified material, Cu–Al-MCM-22, showed a prominent band at around 220 nm as well as a very broad band in the range of 600–850 nm. These peaks are attributed to the ligand-to-metal charge transfer in monomeric Cu^{2+} ions interacting with oxygen in the zeolite crystal lattice ($O^{2-} \rightarrow Cu^{2+}$) and the d–d transition in Cu^{2+} located in distorted octahedral coordination, respectively.[22] Hence, it may be concluded that copper was deposited on the surface of the Al-MCM-22 sample in the form of well-dispersed Cu^{2+} cations. Analysis of the spectra recorded for the Ce–Cu-modified samples is more complicated, due to their similar absorption regions for transitions in cerium and copper in the range of 200–400 nm. Therefore, the broad band with a maximum located at around 225 nm could arise from the superposition of the bands indicating ligand-to-metal charge transfer, such as $O^{2-} \rightarrow Cu^{2+}$ and $O^{2-} \rightarrow Ce^{4+}$. However, the Cu–Ce-MWW derivatives are characterized by a broader absorption region below 400 nm in comparison to the Cu–Al-MCM-22 sample. Therefore, this band broadening could be attributed to the presence of cerium cations in the sample. Nevertheless, based on the analysis of the spectra (Fig. 6C), it can be assumed that copper was deposited mainly in the form of monomeric Cu^{2+} cations. This statement is supported by the presence of the broad band in the range of 600–850 nm, assigned to the d–d transition of Cu^{2+} ions in
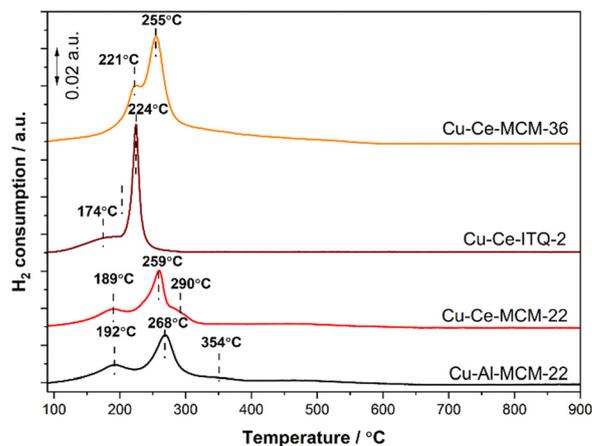
structure.[26] Only for the Ce-MCM-22(P) sample, a small shoulder located at around 430 nm could be related to the presence of more aggregated cerium species.[29] Such forms are not identified for the other two samples, Ce-ITQ-2(P) and Ce-MCM-36(P). It could be connected with their post-synthesis treatments (under basic and then acidic conditions), which could affect the partial removal of cerium species located outside of the zeolite framework. In the case of the spectra recorded for the calcined Ce-MWW samples, Fig. 6B, one broad band with the maximum at around 290 nm can be found. The absorption in this wavelength range is

Fig. 7 H_2-TPR profiles of the Cu-modified Al-MCM-22 and Ce-MWW derivatives.

pseudo-octahedral coordination (*e.g.*, $Cu(H_2O)_6^{2+}$).[34,35] What is more, the presence of these peaks was only confirmed for the copper-modified samples (Fig. 6C), whereas for the Ce-MWW derivatives, no absorption was found in this region (Fig. 6A and B).

The additional information about the form, aggregation and coordination state of the catalyst's active components can be obtained from the temperature-programmed reduction of the samples with hydrogen (H_2-TPR). The thermoreduction profiles of the Cu-modified zeolites are presented in Fig. 7. Their shapes indicate that complete copper reduction occurred below 400 °C. The H_2-TPR profile of Cu–Al-MCM-22 consists of three reduction peaks at around 192, 268 and 354 °C, described as α, β and γ. The first, α peak, can be interpreted as the reduction of monomeric Cu^{2+} cations to Cu^+, whereas the β peak is assigned to the reduction of monomeric Cu^+ cations to Cu^0.[36] The shoulder at around 354 °C is linked with the reduction of bulk CuO species.[37] The low intensity of γ peaks may be related to a small CuO contribution concerning the total copper deposited on the catalyst's surface. It was also evidenced by the results of the P-XRD studies (Fig. 2C, no CuO reflections were found) and UV-vis-DR (Fig. 6C, only the bands characteristic of monomeric copper species were detected). The H_2-TPR profile recorded for the Cu–Ce-MCM-22 sample is comparable to its analogue without cerium. It also has three peaks, although shifted towards lower temperatures. According to literature data,[37] this phenomenon can be related to the synergistic effect occurring between copper and cerium species. The interaction between them affects the enhancement of the mobility of oxygen from the framework due to the weakening of the Ce–O bond strength.[37] The lowest reduction temperatures were evidenced for the Cu–Ce-ITQ-2 sample and are presented in Fig. 7 (α ~ 174 °C and β ~ 224 °C). For this catalyst, both the addition of cerium cations and bimodal porous system, which improves the accessibility of transition metal cations, are responsible for the increased reduction properties. The effect of a more open porous structure of the delaminated sample also prevented the formation of metal oxide aggregates, as evidenced by the absence of the γ reduction peak. In the case of Cu-modified pillared MWW, its thermoreduction profile does not follow the trend of the other samples of the series. The α reduction peak in the profile of Cu–Ce-MCM-36 is located at slightly higher temperatures than its 3D analogue, while the β peak is located at nearly the same temperature as in the profile of Cu–Ce-MCM-22. For this sample also the γ peak was not found. The shape of the H_2-TPR profile recorded for the incompletely intercalated sample may relate to the lower accessibility of the reducing agent to metal cations because of the partial blocking of the pores by amorphous silica aggregates.

The concentration of surface acid sites together with their acidic strength was evaluated using the method of temperature-programmed desorption of ammonia (NH_3-TPD). The profiles of ammonia desorption are presented in Fig. 8,
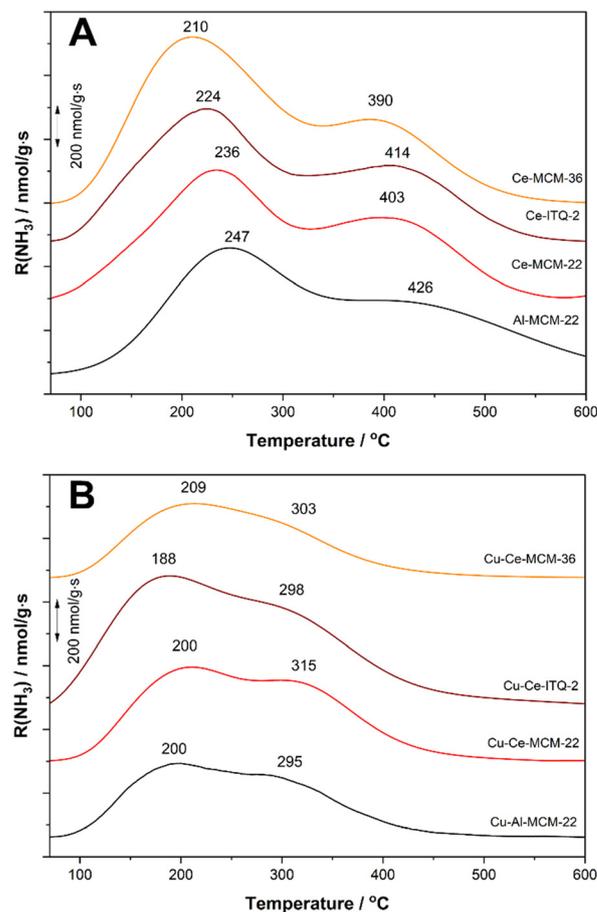

Fig. 8 NH_3-TPD profiles recorded for the Al-MCM-22 and Ce-MWW supports (A) and their copper-modified forms (B).

while the acidic properties of the samples, such as concentration and density of acid sites, were determined and accordingly listed in Table 1. The acidity of the samples depends on their chemical composition and is related to the presence of Brønsted, ≡Si–O(H)–Al≡, and Lewis (aluminum, cerium and copper centres) acid sites. The NH_3-TPD profiles recorded for the MWW-derivatives, Fig. 8A, demonstrate two distinct maxima, in low-temperature and high-temperature ranges. The first maximum, located at around 210–247 °C, is assigned to the centres characterized by weak adsorption of NH_3 onto the catalyst surface, and therefore can be classified as weak acid sites. On the other hand, the high-temperature peak, located at about 390–426 °C, is related to the presence of stronger acid sites. The shape of the ammonia desorption profiles of the Ce-MWW derivatives is similar to the profile of the Al-MCM-22 sample. They consist of two peaks, although their maxima are shifted to lower temperatures. For Ce-MCM-22, the concentration of acid sites (Table 1) is slightly lower compared to its Si–Al-analogue. This phenomenon, related to cerium incorporation into the zeolite framework, was supposed and reported also by other authors.[38] Roth *et al.*[26] stated that the form of cerium is particularly difficult to reveal, especially since they are observed in both Ce^{3+} and

Ce^{4+} framework cations. The presence of cerium in the +4 oxidation state does not provide acidic hydroxyl groups in tetrahedral coordination.[26]

It is also worth mentioning that the densities of acid sites are comparable (Table 1), indicating the equivalent distribution of centres available for ammonia molecule adsorption on the zeolite surface. The results obtained for the micro-mesoporous materials (Ce-ITQ and Ce-MCM-36), presented in Table 1, show that the total concentration of acid sites increased despite the decrease in aluminum and cerium content. Hence, the access of probe molecules to the acid centres was improved as a result of a more open structure of the samples with bimodal porosity (Ce-ITQ-2 and Ce-MCM-36). The high concentration of surface acid sites determined for the pillared sample is surprising, especially in contrast to the delaminated sample. For Ce-MCM-36, one should suspect that its acidic properties will be lower compared to Ce-ITQ-2 due to the introduction of amorphous silica into its inter-layer space, which does not contribute to the total acidity of the samples.[30] Taking into account the abovementioned observation, this explanation may require future more in-depth studies.

The NH_3-TPD profiles of the Cu-containing samples are shown in Fig. 8B. The ammonia desorption profiles obtained for these samples were slightly changed in comparison to zeolites non-modified with metal cations (Fig. 8A), especially taking into consideration the ammonia release temperature. Deposition of copper resulted in the increased contribution of medium-strength acid sites as a result of different aggregations of copper species and consequently different accessibility of probe molecules to the acidic sites. For the Cu-modified catalysts, the positions of ammonia adsorption maxima are shifted to the lower temperature range. A less significant shift of these peaks is observed for the Ce-MCM-36 zeolite functionalised with copper. The lower temperature of ammonia desorption from the catalyst's surface can be related to the formation of the sites with decreased acidic strength. The studies of UV-vis-DR (Fig. 6C) and H_2-TPR (Fig. 7) indicate that copper in all obtained samples was deposited mainly in the form of highly dispersed copper cations. However, for the abovementioned cases, Cu–Al-MCM-22 and Cu–Ce-MCM-22, the presence of small copper oxide aggregates was also identified. The type of surface acidity was changed as a result of Cu^{2+} cation substitution in the ion-exchange positions ($\equiv$Si–O(H)–Al$\equiv$). Therefore, the additional type of acidity, connected with the introduced copper species, plays the role of electron pair acceptors. The concentration and density of surface acid centres for the Cu-modified materials are summarized in Table 1. In general, deposition of transition metals into zeolites resulted in a decreased concentration of surface acid sites. The effect was less significant for the delaminated sample. The Cu–Ce-ITQ-2 sample is characterized by the highest acidity in the Cu-MWW series, both in terms of concentration and density of acid sites. In the case of this catalyst, the accessibility of ammonia molecules to the acid centres is greater than in the

case of other samples. This is related to the more open structure of the delaminated sample, and thus better dispersion of copper species on the zeolite layers resembling a house-of-cards structure. These results are consistent with the results of UV-vis-DR analysis (Fig. 6C) but also with H_2-TPR studies (Fig. 7), regarding copper dispersion and form. For the other samples, the drop in acidic properties could be assigned to the partial blocking of pores by more aggregated copper oxide species. Thus, it may result in the restricted access of NH_3 molecules to both Brønsted ($\equiv$Si–O(H)–Al$\equiv$) and Lewis (aluminum, cerium and copper centres) acid sites.

The MWW derivatives modified with copper by the ion-exchange method were studied as catalysts of the selective catalytic reduction of NO with ammonia (NH_3-SCR) (Fig. 8 and 9). All obtained samples were found to be active and selective catalysts in the NO conversion process. Catalytic tests were performed at two various catalyst loads – gas hourly space velocity (GHSV) of 17 000 and 68 000 h^{-1}. The NO conversion obtained in the presence of Cu–Ce-MWW zeolites, Cu–Ce-MCM-22 and Cu–Ce-MCM-36, was comparable, indicating their very similar activity in the tests conducted with a GHSV of 17 000 h^{-1} (Fig. S2†). The small differences in the catalytic performance of the Cu-modified zeolites with the MWW topology were also described by other authors.[22,39] Thus, it may be possible that the strong interaction between the MWW framework and the copper species deposited on its surface is responsible for the high catalytic activity of this catalytic system in the NH_3-SCR process. Nevertheless, the differences in the catalytic performance among the Cu-modified zeolites were
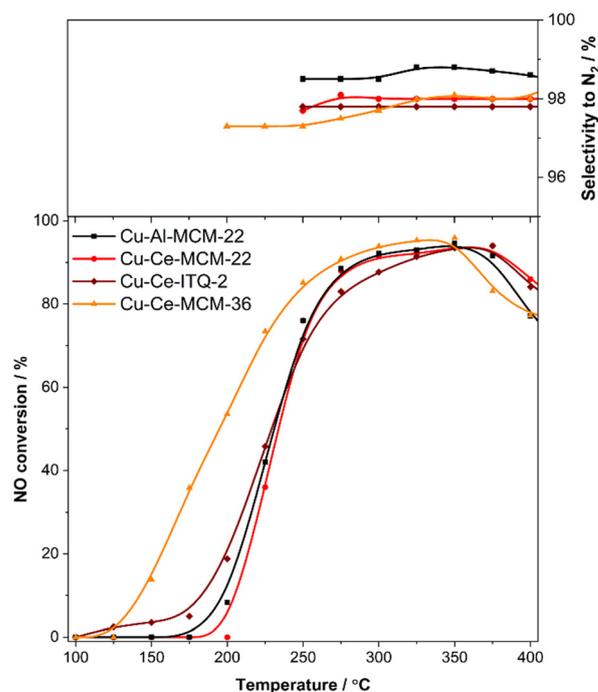

Fig. 9 NH_3-SCR catalytic studies of the Cu-modified Al-MCM-22 and Ce-MWW derivatives (GHSV of 68 000 h^{-1}).

noticeable, especially when GHSV was increased to 68 000 h⁻¹ (Fig. 9). In the case of the most active catalyst of the studied series, Cu–Ce-MCM-36, the NO conversion started at 150 °C and reached its maximum value at the lowest temperature of all the studied catalysts (325 °C). What is more, the delaminated sample (Cu–Ce-ITQ-2) was also characterized by increased NO conversion in the low-temperature range (125–200 °C) in comparison to 3D Cu-modified MWW analogues. For both micro-mesoporous samples, the impact of bimodal porosity is greatly visible at temperatures lower than 200 °C, when the reaction efficiency is not yet very high. Above 200 °C, the NO conversion profiles for the Cu–Al-MCM-22, Cu–Ce-MCM-22 and Cu–Ce-ITQ-2 samples are similar, indicating that diffusion aspects are less important in these temperature ranges. For the Cu–Ce-MCM-36 sample, the increased catalytic activity could be related to the micro-mesoporous system, which guarantees greater accessibility of reactants to catalytically active sites. Moreover, the synergistic effect of copper and cerium resulted in the widening of the operating temperature window for the SCR reaction below 300 °C.[40] Another possible factor influencing the improved catalytic properties of Ce-containing catalysts is improved redox properties of such systems. As it was already discussed, the copper–cerium-MWW samples exhibited extraordinary surface reducibility (H₂-TPR profiles, Fig. 7). According to Z. Liu et al.[41] the redox properties of catalysts are crucial for the NH₃-SCR catalytic activity. The redox cycle: $Cu^{2+} + Ce^{3+} \leftrightarrow Cu^+ + Ce^{4+}$, leads to a reduction in the energy needed for electron transfer between catalyst components, activating ammonia and nitrogen(II) oxide molecules into catalytic conversion.[41] Consequently, this system promotes the transfer of electrons and enhances the NO conversion over the Cu–Ce-containing catalysts.[42]

The results of catalytic activity tests, in terms of the NO conversion, carried out for increased GHSV (68 000 h⁻¹) were reduced compared to 4 times the lower value of GHSV (17 000 h⁻¹). In the tests conducted with a GHSV of 68 000 h⁻¹, lower NO conversion values in the higher temperature range were achieved compared to catalytic tests performed with a GHSV of 17 000 h⁻¹. The comparison of the catalyst performance of Cu–Ce-MCM-22 and Cu-Ce-MCM-36 showed the largest difference in catalytic activity for different GHSVs as presented in Fig. 10. In the case of the tests performed with a GHSV of 17 000 h⁻¹, the reaction was started at about 125 °C for Cu–Ce-MCM-36 (Fig. 10B), while in the case of the Cu-Ce-MCM-22 sample (Fig. 10A), the process was initiated at a temperature higher by about 25 °C. Then, almost 100% of the NO conversion was reached at around 225–250 °C and remained steadily high until 375 °C. At higher temperatures (<375 °C) the side process of direct ammonia oxidation, resulting in a decrease in NO conversion, was observed.[43] Such catalytic performance was described by other authors as typical for Cu-modified zeolites with MWW topology.[39] The selectivity to N₂ for both samples was very high and exceeded 98% within the whole studied temperature range.
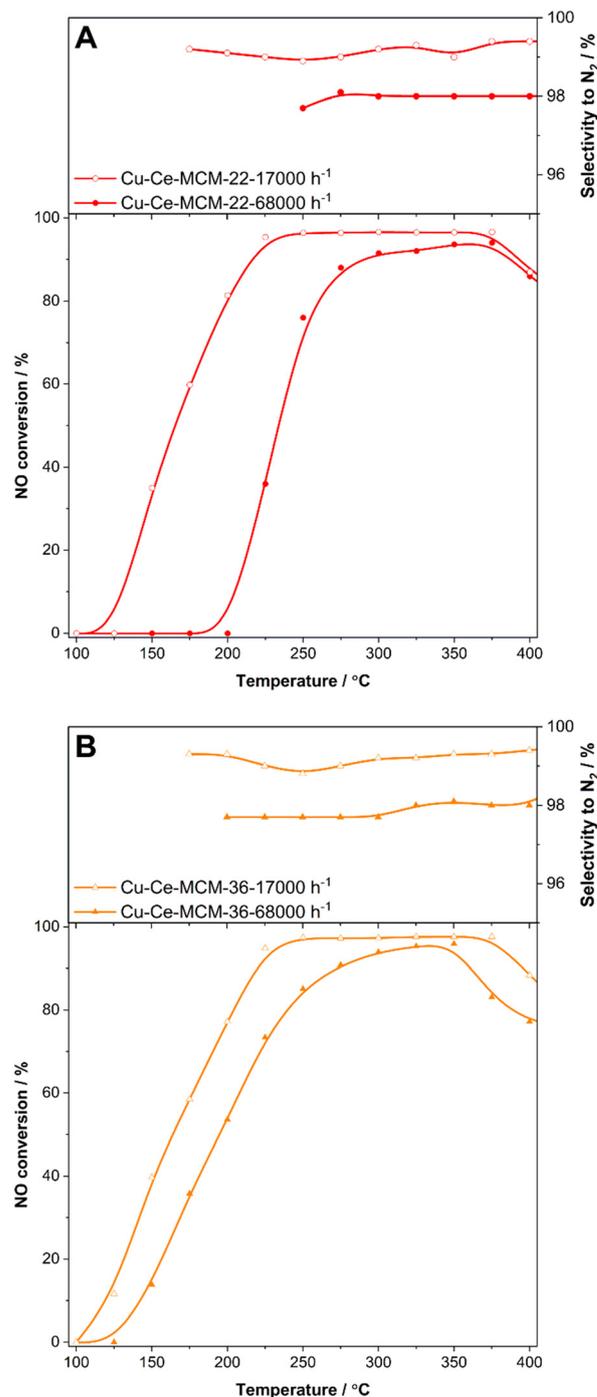

Fig. 10 Temperature dependence of catalytic NH₃–SCR activity: (A) Cu–Ce-MCM-22 and (B) Cu–Ce-MCM-36 catalysts with various GHSVs.

Copper introduced into the Al-MCM-22 and Ce-MWW derivatives was present mainly in the form of well-dispersed copper species, as was proved by UV-vis-DR (Fig. 5C) and H₂-TPR (Fig. 7) measurements. Such copper forms were found to be more active in NO to NO₂ oxidation compared to aggregated copper oxide species.[44] The presence of nitrogen(IV) oxide is necessary for the low-temperature conversion of NOₓ according to the fast-SCR mechanism,
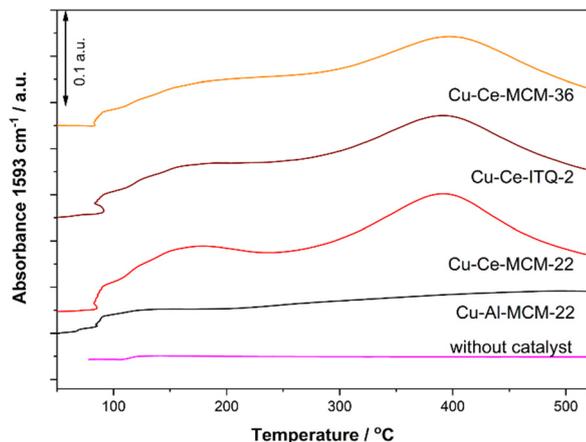
This journal is © The Royal Society of Chemistry 2025

Catal. Sci. Technol., 2025, **15**, 1456–1472 | **1467**

Fig. 11 NO to NO_2 oxidation studies in the presence of the Cu-modified Al-MCM-22 and Ce-MWW derivatives.

Fig. 12 Ammonia oxidation catalytic studies of the Cu-modified Al-MCM-22 and Ce-MWW derivatives (GHSV of 68 000 h^{-1}).

$2NH_3 + NO + NO_2 \rightarrow 2N_2 + 3H_2O$.[44] To verify the possible role of the fast-SCR mechanism, the obtained catalysts were tested in the NO to NO_2 oxidation process, based on the analysis of the FTIR band at 1593 cm^{-1} characteristic of NO_2 formation (Fig. 11). In the case of measurement conducted in the absence of a catalyst, only a small amount of NO_2 was detected – about 2–2.5% of NO-to-NO_2 conversion was observed. In turn, such a test reaction in the presence of the studied catalysts resulted in significantly higher NO to NO_2 conversion. The NO conversion is significantly higher for the Ce-MWW catalysts than for the Cu–Al-MCM-22 sample (Fig. 11). According to Guo et al.,[45] incorporating Ce would enhance the NO oxidation efficiency compared to catalysts containing copper, thereby promoting the acceleration of the SCR reaction. The nitrogen(IV) oxide formation started directly after introducing the reaction mixture into the reactor at around 100 °C. Then, the NO conversion remained constant until about 250 °C. Above 250 °C intensified production of NO_2 was observed, reaching the maximum at 390–400 °C. The decrease in NO_2 evolution at higher temperatures is related to the thermodynamic limitations of exothermic reversible oxidation of NO to NO_2.[46] The described process of NO_2 formation could be one of the main factors affecting the increased low-temperature NH_3-SCR efficiency.

The catalytic performance of the zeolitic catalysts in the side process of direct ammonia oxidation (NH_3ox) was verified in an additional experiment. The results of these studies are presented in Fig. 12 and S2.† As previously mentioned, the drop in NO conversion observed above 375 °C (Fig. 8 and 9) can be attributed to the direct oxidation of ammonia, which plays the role of reducing agent in the NH_3-SCR process. Direct ammonia oxidation is a competitive reaction to the reduction of NO with NH_3 and dominates in the high-temperature range. In order to verify this hypothesis, the reaction of ammonia oxidation was tested for two different GHSV values of 17 000 (Fig. S3†) and 68 000 h^{-1} (Fig. 12). The well-visible differences in the catalytic performance of the
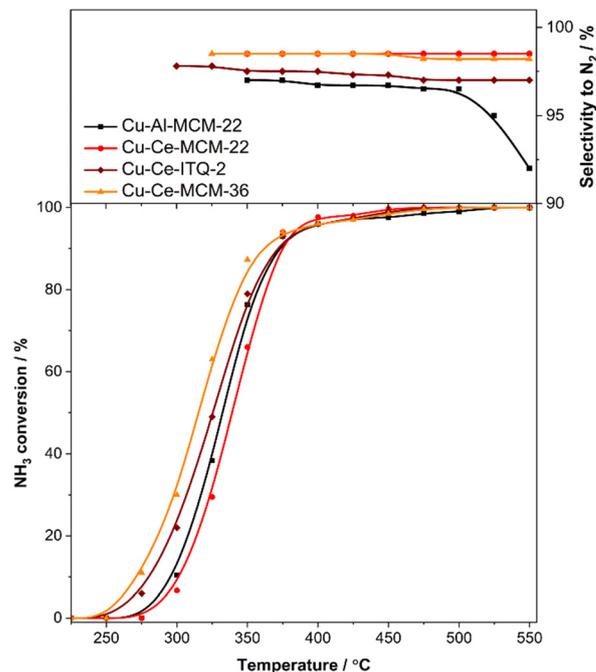
studied samples are presented for the NH_3ox studies under a GHSV of 68 000 h^{-1}. The studied catalysts presented the following order of NH_3ox efficiency: Cu–Ce-MCM-36 > Cu–Ce-ITQ-2 > Cu–Al-MCM-22 > Cu–Ce-MCM-22. Thus, also in the case of the ammonia oxidation process, the more open structure of the zeolitic material results in improved reaction efficiency. In the case of the test conducted with a GHSV of 17 000 h^{-1} (Fig. S4†), the reaction started at about 275 °C and the ammonia conversion reached nearly 100% above 350 °C. For both studied reaction conditions (GHSV of 68 000 and 17 000 h^{-1}, Fig. 11 and S2†) the most active catalyst in NH_3 oxidation was Cu–Ce-MCM-36. The results of ammonia oxidation clearly show that a decrease in NO conversion above 375 °C (Fig. 9) was attributed to the intensified direct oxidation of ammonia.

The comparison of the polythermal NH_3-SCR catalytic tests conducted in the flow of dry and wet reaction mixtures in the presence of copper-modified zeolites is presented in Fig. 12 and S3.† The catalytic studies were performed for a GHSV of 17 000 h^{-1} in the humid reaction mixture (5 vol% H_2O). A decrease in the catalytic activity was observed for all the catalysts under these reaction conditions. The drop in NO conversion over the Cu-modified zeolites could be related to the competitive chemisorption of ammonia and water molecules on the same adsorption sites. Analogous results were also reported for similar catalytic systems, such as layered ferrierites functionalised with copper species.[47,48]

The commercial catalytic system used for the treatment of the NO_x-containing gasses emitted from stationary sources, e.g., power plants, is based on the V_2O_5–TiO_2 system.[48] This vanadia–titania catalyst operates in a relatively narrow range

1468 | Catal. Sci. Technol., 2025, **15**, 1456–1472

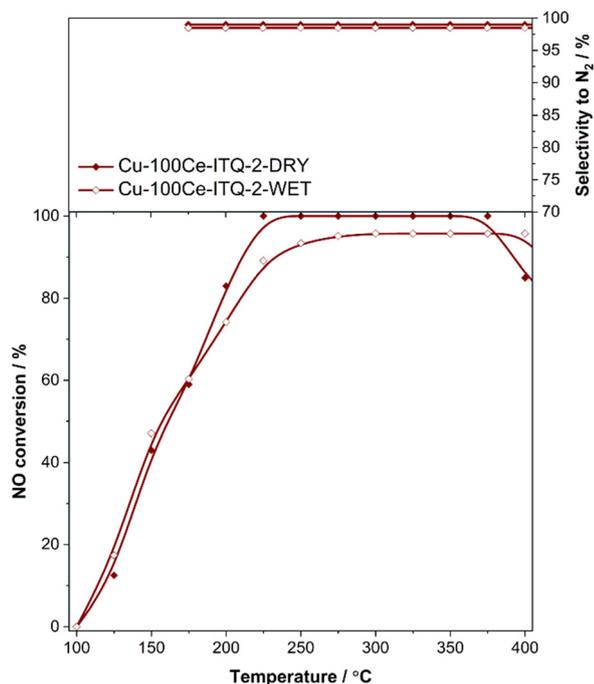This journal is © The Royal Society of Chemistry 2025

Fig. 13 Temperature dependence of catalytic NH$_3$-SCR activity of the Cu-Ce-ITQ-2 catalyst under dry and humid (5 vol% H$_2$O) conditions (GHSV of 17 000 h^{-1}).

Fig. 14 Long-term NH$_3$-SCR performance of the Cu-100-ITQ-2 catalyst and 5 vol% H$_2$O resistance at 225 °C (GHSV of 17 000 h^{-1}).

of temperatures, 300–400 °C. The most active sample under humid reaction conditions, Cu–Ce-ITQ-2, reached about 100% nitrogen(II) oxide conversion in the wide temperature range of 225 to 375 °C with a N$_2$-selectivity above 97% (Fig. 13). In the case of the obtained catalysts, the window of the effective NO conversion was extended and strongly shifted towards lower temperatures in comparison to the commercial V$_2$O$_5$–TiO$_2$-based catalyst.[48] Therefore, the obtained Cu–Ce-ITQ-2 system meets the requirements of modern low-temperature NH$_3$-SCR installations and operates with a good efficiency below 300 °C. The most active catalyst can be considered as an alternative for possible application in low-temperature retrofitted NH$_3$-SCR installations. Therefore, this catalyst was tested in various stability catalytic tests, including long-term NH$_3$-SCR studies as well as durability in the wet reaction mixture (Fig. 13).

Fig. 14 shows the results of the 20-hour NH$_3$-SCR stability catalytic tests for the Cu–Ce-ITQ-2 catalyst. The isothermal tests were conducted at 225 °C in the flow of dry and wet (5 vol% of water vapour) reaction mixture. During the first three hours of the reaction under dry conditions, the NO conversion decreased from 95 to 93%. Then, for the next 12 h, the NO conversion was stable, and finally, the conversion decreased to about 92%. However, for the last three hours of the experiment, the NO conversion once again increased to reach 94%. The selectivity to N$_2$ was high (above 98%) and did not change significantly during the NH$_3$-SCR test. It is worth mentioning that the changes in the catalytic activity of the Cu-ITQ-2 sample after 20 h of the reactions were rather small, therefore the tested catalyst can be considered as
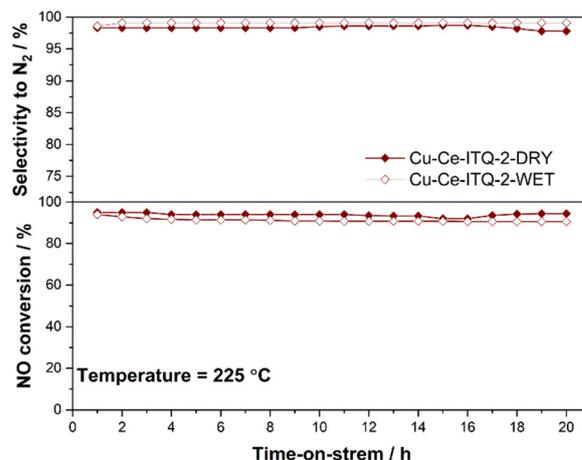
stable, both in terms of NO conversion and selectivity to N$_2$. In the case of the stability tests under wet reaction mixture conditions, Cu-ITQ-2-WET (Fig. 14), the changes in activity and selectivity of the studied catalyst were rather small. Therefore, the obtained results were promising for the potential application of such catalytic systems in low-temperature NO$_x$ conversion.

The Cu–Ce-ITQ-2 catalyst after catalytic studies with the wet reaction mixture (Fig. 14) was analysed with respect to forms and aggregation of copper species by UV-vis-DR and P-XRD. These results are presented in the ESI, Fig. S5 and S6,† respectively. The UV-vis-DR spectra recorded for the copper-modified delaminated zeolite before and after the catalytic test are very similar (Fig. S5†) and indicate the presence of copper mainly in the form of isolated cations. However, for the sample after stability studies a shoulder at around 340 nm in the absorption region characteristic of oligomeric copper species can be found. Therefore, some of the copper cations could be transformed into slightly more aggregated oligomeric copper oxide species. In the case of the diffractogram recorded for the used catalysts, no reflections characteristic of the CuO phase were found (Fig. S6†). Therefore, it can be concluded that the sample's physicochemical characteristics did not change significantly after catalytic reactions. Thus, the tested catalyst, Cu–Ce-ITQ-2, is stable under reaction conditions and seems to be a promising material for possible low-temperature NO$_x$ conversion in the NH$_3$-SCR process.

The core of modern NH$_3$-SCR studies is based on the appropriate choice and then design of catalysts, which can be broadly classified into three main categories: noble metal catalysts, transition metal oxide catalysts, and zeolite-based catalysts. Undoubtedly, each category has its advantages and disadvantages concerning issues such as catalytic efficiency, stability, and cost-effectiveness.[49] Taking into account the first group mentioned before, they demonstrate excellent catalytic activity at low temperatures, but on the other hand, noble metal-based catalysts face challenges such as

This journal is © The Royal Society of Chemistry 2025

Catal. Sci. Technol., 2025, **15**, 1456–1472 | **1469**

Table 2 Comparison of Cu–Ce-MWW series' 90% NO_x conversion with other catalyst types

Catalyst name	NO_X conversion	GHSV [h^{-1}]	Reference
Cu–Ce-MWW	200–375 °C (>90%)	17 000	—
Cu-SSZ-13	225–300 °C (>90%)	20 000	51
CeCrCu/TiO2	250–400 °C (>90%)	20 000	52
@CuMgAl-MOs	250–350 °C (~80%)	12 000	53
CeVO$_x$/AC	180–200 °C (>90%)	12 000	54
Cu-M41S	250–350 °C (>90%)	12 000	55

insufficient thermal stability, low N_2-selectivity, and high costs, which significantly limit their practical applications.[49] Among the previously described categories, the high price of such noble metal systems is the factor that drives research to find cheaper and in many cases better alternatives for use in low-temperature NO_x conversion. This does not change the fact that the NO conversion rates that can be obtained in the presence of Pt-containing catalysts reach about 80% at a temperature of about 180 °C (GHSV = 24 000 h^{-1}).[50]

The temperature window of effective operation of the obtained catalysts was compared with other catalytic materials reported in the recent literature (Table 2). Materials such as modified: zeolites,[51] TiO_2,[52] double layered hydrotalcites,[53] activated carbon,[54] and mesoporous silicas[55] were taken into account, while the parameters of the catalytic reaction were similar to those used in the presented studies (~17 000 h^{-1}). The 90% NO_x conversion reached for the Cu-modified zeolites with the MWW topology was obtained in the range of 200–375 °C. Comparing the obtained results with literature data, the Cu–Ce-MWW materials are characterized by a wide temperature window of effective operation. Only the catalysts based on modified activated carbons were reported to operate at lower temperatures, although such catalysts are effectively operated in a very narrow temperature range of 180–200 °C. Therefore, the obtained catalysts are classified as an interesting and promising group of catalytic materials for the low-temperature NH_3-SCR process.

Conclusions

The Al-MCM-22 and Ce-MCM-22 samples and their Ce-containing derivatives with bimodal porosity, house-of-cards structure zeolite (Ce-ITQ-2) and silica pillared MWW derivative (Ce-MCM-36), were successfully obtained. The catalytic activation of these materials to the NH_3-SCR process included deposition of copper species, mainly copper cations, by the ion-exchange method. As a result of such modifications, catalysts active and selective in the low-temperature NH_3-SCR process were obtained. The positive effect of the structure opening on the catalytic activity of the samples was observed for the catalytic tests conducted with increased space velocity (GHSV). The silica intercalated and copper-modified sample, Cu–Ce-MCM-36, showed the highest catalytic performance among the studied catalysts, possibly

due to the decreased diffusion limitations in the pores. In the case of the catalytic tests conducted with a GSHV of 17 000 h^{-1}, the temperature region of the effective catalytic operation was in the range of 225–375 °C and was shifted towards lower temperatures in comparison to the commercial V_2O_5–TiO_2 system. In the case of the Ce-zeolites synthesized by a one-pot procedure, cerium cations were successfully incorporated into the MWW matrix, which was confirmed by FTIR and UV-vis-DR measurements. Copper deposited into the zeolitic samples by the ion-exchange method was present mainly in the form of monomeric Cu^{2+} cations. The interaction between Cu–Ce was reflected by the enhancement of oxygen mobility from the framework due to the weakening of the Ce–O bond strength and resulted in decreased reduction temperature of copper species. What is more, the cerium introduction into the zeolite structure improved the effectiveness of NO oxidation to NO_2 compared to silica–alumina catalysts containing copper, thereby promoting the acceleration of NO_x conversion by the fast-SCR pathway. The micro-mesoporous catalyst, Cu-ITQ-2, presented high catalytic stability both under dry and wet reaction conditions. Its increased catalytic performance in the studied series of catalysts could be connected with various factors, especially the open structure of the delaminated zeolites as well as copper–cerium synergistic cooperation.

Data availability

The datasets supporting this article have been deposited at RODBUK Cracow Open Research Data Repository under doi: **https://doi.org/10.57903/UJ/MZIWEX**.

Author contributions

Conceptualization: A. J. and L. C.; methodology: A. J. and L. C.; investigation: A. J., K. F., M. R., A. K. and M. M.; writing: A. J.; original draft preparation: A. J.; writing–review and editing: M. R. and L. C.; visualization: A. J.; supervision: L. C. All authors have read and agreed to the published version of the manuscript.

Conflicts of interest

There are no conflicts to declare.

Acknowledgements

References

1 T. Boningari and P. G. Smirniotis, *Curr. Opin. Chem. Eng.*, 2016, **13**, 133–141.
2 N. Usberti, M. Jablonska, M. Di Blasi, P. Forzatti, L. Lietti and A. Beretta, *Appl. Catal., B*, 2015, **179**, 185–195.

1470 | *Catal. Sci. Technol.*, 2025, **15**, 1456–1472

This journal is © The Royal Society of Chemistry 2025

3   Z. Shi, Q. Peng, E. Jiaqiang, B. Xie, J. Wei, R. Yin and G. Fu, *Fuel*, 2023, **331**, 125885.

4   D. Damma, P. R. Ettireddy, B. M. Reddy and P. G. Smirniotis, *Catalysts*, 2019, **9**, 349.

5   Z. Sun, X. Mi, Y. Luo, S. Wang, B. Yuan, R. Hao and Y. Zhao, *ACS Omega*, 2021, **6**, 34347–34358.

6   W. Liu, Y. Long, X. Tong, Y. Yin, X. Li and J. Hu, *Mol. Catal.*, 2021, **515**, 111888.

7   M. Rutkowska and L. Chmielarz, *Catalysts*, 2024, **14**(5), 290.

8   S. S. R. Putluru, L. Schill, A. D. Jensen and R. S. N. Fehrmann, *J. Chem.*, 2018, **2018**, 8614747.

9   K. A. Tarach, M. Jablonska, K. Pyra, M. Liebau, B. Reiprich, R. Glaser and K. Gora-Marek, *Appl. Catal., B*, 2021, **284**, 119752.

10 Q. Liu, C. Bian, S. Ming, L. Guo, S. Zhang, L. Pang, P. Liu, Z. Chena and T. Li, *Appl. Catal., A*, 2020, **607**, 117865.

11 N. C. Nelson, T. Andana, K. G. Rappé and Y. Wang, *Catal. Sci. Technol.*, 2023, **13**(4), 1111–1118.

12 J. Wang, Z. Peng, H. Qiao, H. Yu, Y. Hu, L. Chang and W. Bao, *Ind. Eng. Chem. Res.*, 2016, **55**, 1174–1182.

13 Y. Cao, L. Lan, X. Feng, Z. Z. Yang, S. Zou, H. D. Xu, Z. Q. Li, M. C. Gong and Y. Q. Chen, *Catal. Sci. Technol.*, 2015, **5**(9), 4511–4521.

14 S. J. Deng, D. D. He, Z. H. Wang, Z. P. Chen, Y. Ji, G. P. Yan, G. J. Hou, L. C. Liu and H. J. He, *J. Rare Earths*, 2021, **39**, 969–978.

15 Q. Wu, C. Fan, Y. Wang, X. Chen, G. Wang, Z. Qin, S. Mintova, J. Li and J. Chen, *Chem. Eng. J.*, 2022, **435**, 134890.

16 Y. Lyu, G. Lyu, R. Sun and C. Song, *Fuel*, 2024, **367**, 131456.

17 J. Yang, Z. F. Li, J. X. Cui, Y. Y. Ma, Y. Y. Li, Q. Zhang, K. Song and C. L. Yang, *J. Rare Earths*, 2023, **41**, 1195–1202.

18 A. Jankowska, J. Ciuba, A. Kowalczyk, M. Rutkowska, Z. Piwowarska, M. Michalik and L. Chmielarz, *Catal. Today*, 2022, **390-391**, 281–294.

19 S. Narayanan, P. Tamizhdurai, V. L. Mangesh, C. Ragupathi, P. S. Krishnan and A. Ramesh, *RSC Adv.*, 2021, **11**(1), 250–267.

20 J. Čejka and B. Wichterlová, *Catal. Rev.: Sci. Eng.*, 2002, **44**, 375–421.

21 U. Díaz, *ISRN Chem. Eng.*, 2012, **2012**, 1–35.

22 M. Rutkowska, U. Díaz, A. E. Palomares and L. Chmielarz, *Appl. Catal., B*, 2015, **168–169**, 531–539.

23 A. Jankowska, A. Kowalczyk, M. Rutkowska, W. Mozgawa, B. Gil and L. Chmielarz, *Catal. Sci. Technol.*, 2020, **10**(23), 7940–7954.

24 A. Szymaszek-Wawryca, U. Díaz, B. Samojeden and M. Motak, *Molecules*, 2022, **27**(9), 2983.

25 A. Corma, C. Corell and J. Pérez-Pariente, *Zeolites*, 1995, **15**(1), 2–8.

26 W. J. Roth, B. Gil, W. Makowski, A. Sławek, A. Korzeniowska, J. Grzybek, M. Siweka and P. Michorczyk, *Catal. Sci. Technol.*, 2016, **6**(8), 2742–2753.

27 U. Díaz, V. Fornés and A. Corma, *Microporous Mesoporous Mater.*, 2006, **90**(1), 73–80.

28 A. Corma, C. Corell, V. Fornés, W. Kolodziejski and J. Pérez-Pariente, *Zeolites*, 1995, **15**(7), 576–582.

29 Y. Wu, J. Wang, P. Liu, W. Zhang, J. Gu and X. Wang, *J. Am. Chem. Soc.*, 2010, **132**(51), 17989–17991.

30 M. Marosz, B. Samojeden, A. Kowalczyk, M. Rutkowska, M. Motak, U. Diaz, A. E. Palomares and L. Chmielarz, *Materials*, 2020, **13**, 2399.

31 M. Thommes, K. Kaneko, A. V. Neimark, J. P. Olivier, F. Rodriguez-Reinoso, J. Rouquerol and K. S. W. Sing, *Pure Appl. Chem.*, 2015, **87**, 1051.

32 J. S. S. Lowell, M. A. Tomas and M. Thommes, *Characterization of Porous Solids and Powders: Surface Area, Pore Size and Density*, Springer, Netherlands, 2004.

33 S. C. Laha, P. Mukherjee, S. R. Sainkar and R. Kumar, *J. Catal.*, 2002, **207**(2), 213–223.

34 L. Martins, R. P. S. Peguin, M. Wallau and G. A. Urquieta, *Stud. Surf. Sci. Catal.*, 2004, **154**, 2475–2483.

35 M. Rutkowska, Z. Piwowarska, E. Micek and L. Chmielarz, *Microporous Mesoporous Mater.*, 2015, **209**, 54–65.

36 Y. Hu, L. Dong, M. Shen, D. Liu, J. Wang, W. Ding and Y. Chen, *Appl. Catal., B*, 2001, **31**(1), 61–69.

37 F. Zhao, S. Li, X. Wu, R. Yue, W. Li, X. Zha, Y. Deng and Y. Chen, *Catalysts*, 2019, **9**, 256.

38 M. Sedighi, M. Ghasemi and A. Jahangiri, *Korean J. Chem. Eng.*, 2017, **34**, 997–1003.

39 J. Chen, G. Peng, T. Liang, W. Zhang, W. Zheng, H. Zhao, L. Guo and X. Wu, *Nanomaterials*, 2020, **10**, 2170.

40 W. Zhang, Y. Tang, C. Lu, J. Zou, M. Ruan, Y. Yin, M. Qing and Q. Song, *Ultrason. Sonochem.*, 2021, **72**, 105466.

41 Z. Liu, Y. Yi, J. Li, S. I. Woo, B. Wang, X. Cao and Z. Li, *Chem. Commun.*, 2013, **49**, 7726–7728.

42 J. W. Shi, Y. Wang, R. Duan, C. Gao, B. Wang, C. He and C. Niu, *Catal. Sci. Technol.*, 2019, **9**(3), 718–730.

43 B. Pereda-Ayo, U. De La Torre, M. J. Illán-Gómez, A. Bueno-López and J. R. González-Velasco, *Appl. Catal., A*, 2014, **147**, 420–428.

44 A. Święs, A. Kowalczyk, M. Rutkowska, U. Díaz, A. E. Palomares and L. Chmielarz, *Catalysts*, 2020, **10**(7), 734.

45 D. Guo, R. Guo, C. Duan, Y. Liu, G. Wu, Y. Qin and W. Pan, *Mol. Catal.*, 2021, **502**, 111392.

46 G. Qi and W. Li, *Catal. Today*, 2015, **258**, 205–213.

47 A. Święs, A. Kowalczyk, M. Michalik, U. Díaz, A. E. Palomares and L. Chmielarz, *RSC Adv.*, 2021, **11**(18), 10847–10859.

48 L. Chmielarz and A. Jankowska, in *Recent Highlights II*, ed. R. van Eldik and C. D. Hubbard, Academic Press, Cambridge, MA, USA, 2018, vol. 6, pp. 323–383.

49 J. Liu, D. Lv, Y. Wang, Y. Zhao, G. Li and G. Zhang, *ChemCatChem*, 2024, **16**(21), e202301662.

50 A. Valtanen, M. Huuhtanen, A.-R. Rautio, T. Kolli, K. Kordás and R. L. Keiski, *Top. Catal.*, 2015, **58**, 984–992.

51 S. Li, C. Zhang, A. Zhou, Y. Li, P. Yin, C. Mu and J. Xu, *Adv. Mech. Eng.*, 2021, **13**, 16878140211010648.

This journal is © The Royal Society of Chemistry 2025

Catal. Sci. Technol., 2025, **15**, 1456–1472 | **1471**

52 G. Mu, S. Liu, Q. Liu, S. Liu and X. Zhang, *ACS Omega*, 2022, **7**(42), 37694–37704.

53 T. Kondratowicz, O. Horky, S. Slang, L. Dubnova, M. Gajewska, L. Chmielarz and L. Capek, *Nanoscale Adv.*, 2023, **5**(11), 3063–3074.

54 Q. Li, M. Liang, X. Han, Y. Hou and Z. Huang, *J. Hazard. Mater.*, 2022, **424**, 127397.

55 A. Pietraszek, A. Kowalczyk, Z. Piwowarska, M. Rutkowska, O. Iwaszko and L. Chmielarz, *React. Kinet., Mech. Catal.*, 2023, **136**(4), 2259–2276.